Colloid Polym Sci (2002) 280: 857–864
DOI 10.1007/s00396-002-0694-z

ORIGINAL CONTRIBUTION

Augusto Teruo Morita
Danilo Justino Carastan
Nicole Raymonde Demarquette

Influence of drop volume on surface tension evaluated using the pendant drop method

Received: 19 December 2001
Accepted: 5 March 2002
Published online: 29 May 2002

A.T. Morita · D.J. Carastan
N.R. Demarquette (✉)
University of São Paulo – Materials and Metallurgical Engineering Department,
Av. Prof. Mello Moraes 2463,
05508-900 São Paulo, Brazil
E-mail: nick@usp.br
Tel.: +55-11-30915693
Fax: +55-11-30915241

Abstract The pendant drop technique is one of the most accurate methods to measure surface tension of liquids. Recently, it has been found that the value of the surface/interfacial tension found using the pendant drop method might be drop-volume dependent. In this work, the surface tension of glycerol at a 25 °C and the surface tension of polypropylene at 240 °C were measured using the pendant drop method for different drop volumes. It was shown that the values of the surface tension depend on the drop size if no calibration to take into account the anisotropy in the optical enlargement is performed. However, when a calibration procedure for optical anisotropy correction is performed, the values of the surface tension obtained do not depend on the volume drop size and they corroborate the values in the literature.

Keywords Surface tension · Pendant drop method · Volume drop effect · Glycerol · Polypropylene

Introduction

The pendant drop method is probably one of the most popular methods used to measure surface and interfacial tension of liquids. It is an absolute method, independent of contact angle and the experimental setup is fairly simple. It has been used extensively for the evaluation of the surface tension of polymers [1, 2, 3, 4, 5, 6, 7, 8, 9, 10, 11, 12, 13, 14, 15, 16], liquid crystals [17, 18, 19, 20], and other low-molar-mass liquids [21, 22, 23, 24]. The pendant drop method involves the determination of the profile of a drop of one denser liquid suspended in another liquid at mechanical equilibrium. The balance between gravity and surface forces determines the profile of the drop. Recent progress in image analysis and data acquisition systems has made it possible to obtain direct digitization of the drop image with the aid of a video frame grabber of a digital camera [11, 13, 24]. The digital signals are further analyzed using different algorithms to determine the surface/interfacial tension from the drop profile [16, 24, 25, 26, 27].

The equation of Bashforth and Adams [28], which is based on Laplace's equation, relates the drop profile to the surface/interfacial tension through a nonlinear differential equation,

$$\frac{1}{\mathrm{R}\frac{1}{a}} + \frac{\sin\phi}{\frac{x}{a}} = -B\frac{z}{a} + 2, \tag{1}$$

where B, the shape factor of the drop, is given by

$$B = -\frac{a^2 g \Delta\rho}{\gamma}, \tag{2}$$

where $\Delta\rho$ is the difference between the densities of the two liquids in contact (liquid/air in the case of surface tension), g is the gravitational constant, γ is the surface/interfacial tension, a is the radius of curvature at the apex of the drop, x, z, and Φ are the coordinates defined as in Fig. 1, and R_1 is the radius of curvature at the point with coordinates (x,z).

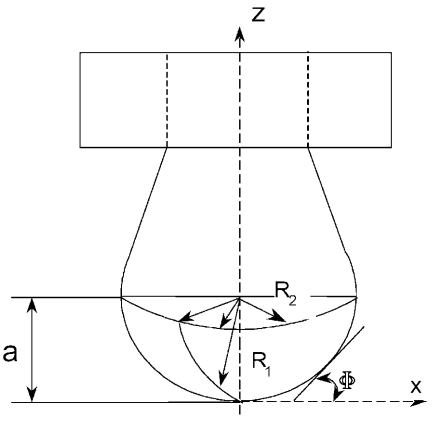

Fig. 1. Pendant drop geometry

R_1 and Φ can be defined geometrically by

$$R_1 = \frac{ds}{d\phi} = \frac{\left[1 + (dz/dx)^2\right]^{3/2}}{d^2z/dx^2} \tag{3}$$

and

$$\sin\phi = \frac{dz/dx}{\left[1+(dz/dx)^2\right]^{1/2}}. \tag{4}$$

The equation of Bashforth and Adams is a second-order nonlinear differential equation between x and z relating the drop profile to the surface/interfacial tension and the difference in the density between the two liquids. This equation is insoluble analytically. Several methods have been developed to extract the surface/interfacial tension from the drop shape [1, 2, 3, 16, 24, 25, 26, 27, 28, 29, 30]. Until the beginning of the 1980s, most of the methods were based on the determination of empirical relations between the shape factor B and dimensionless geometrical quantities of the pendant drop profile [29, 30, 31, 32, 33, 34]. Unfortunately, these methods use only a few experimental points to define the entire shape of the drop, leading to imprecision in the comparison between the experimental profile and the numerical solution of the Bashforth and Adam equation. In the last 20 years, many algorithms to infer the surface/interfacial tension from the profile of a pendant drop have been developed [16, 24, 25, 26, 30, 35, 36, 37, 38, 39]. Some of the most popular algorithms are those of Kwok et al. [16], Voigt et al. [24], and Rotenberg et al. [25], who developed an axisymmetric drop shape analysis that can be used to infer the surface/interfacial tension from the profile of a pendant or a sessile drop [16, 40], the contact angle from the volume and the diameter of sessile drop [16, 41, 42, 43, 44, 45], the surface/interfacial tension and the density from the height, the diameter, and the volume of a sessile drop [40, 46] and the ones of Jennings and Pallas [26] and Pallas and Harrison [47]. Basically, both types of algorithm rely on the comparison between the experimental profile of the pendant drop and a theoretical one obtained by numerical integration of Laplace's equation and on the evaluation of the discrepancy between both curves.

Because of its versatility, the method has long been a source of fascination to engineers, physicists, and mathematicians and a number of articles have been devoted to the improvement of the method. In particular, the influence of drop tilt [17, 48], correction for aspect ratio [17], limit chosen for edge detection [18], illumination [18], syringe diameter [26, 49], necking and capillary effect [4], and accuracy on the surface and interfacial tension inferred have been studied carefully.

According to Bashforth and Adams, surface/interfacial tension measurements are independent of drop volume. However, there is still some controversy in the experimental results published on the effect of the drop volume on the value of the surface/interfacial tension inferred from the profile of a pendant drop. While Demarquette and Kamal [4] and Adão et al. [50] did not observe the influence of the drop volume on the interfacial tension between polystyrene and polypropylene at 230 °C and between water and 1-bromonaphtalene (if the pendant drop was formed by water), Lin and coworkers [27, 49, 51] observed that a reduction in the drop volume below the maximum drop volume of a drop for a specific syringe diameter results in an exponential decrease in the value of the surface/interfacial tension obtained by the analysis of the profile of a pendant drop.

In this work, the effect of the drop volume on the surface tension of glycerol at 25 °C and polypropylene at 240 °C inferred from the analysis of a pendant drop profile is studied. Those liquids were chosen because of the large difference between their surface tensions. In the following sections, the experimental procedures and the calculation methods used to infer the surface/interfacial tension from the drop profile are described, the experimental results of the influence of the drop volume are presented and discussed, and the findings of this work are summarized.

Experimental and evaluation of surface tension

Materials

The surface tension of glycerol from Icar Company (purity 99%) at 25 °C and polypropylene from Polibrasil at 240 °C were evaluated using the pendant drop method for different drop volumes. The densities of glycerol at 25 °C and polypropylene at 240 °C necessary for the calculation of the surface tension were taken as 1.1745 and 0.732 gcm^{-3}, respectively [4, 52].

Pendant drop measurements

The apparatus used in this work was very similar to that used by Demarquette and Kamal [4]. It consists of three parts: an experi-

mental cell where the pendant drop is formed, an optical system to monitor the evolution of the drop, and a data acquisition system to infer the surface tension from the geometrical profile of the drop. The whole system was mounted on a vibration-proof table. This was very important in the case of glycerol, because any vibration of the table would result in the detachment of the drop and in inaccuracy of the detection of the edge of the drop. When experiments with polypropylene were performed, a temperature controller was used to maintain the sample at 240 °C and an argon atmosphere was used in the experimental chamber to avoid thermal degradation of the polymer as the time for the drop to reach mechanical equilibrium could be up to several hours. The needle used for the drops of glycerol was 18 gauge with an inside diameter of 1.3 mm and an outside diameter of 1.8 mm. A special syringe [4] to avoid necking and capillary effects was used to make the pendant drop of polypropylene. The needle used with this syringe was also 18 gauge.

In order to study the influence of the drop volume on the surface tension of glycerol, drops of different volumes were formed in the camera. Images of the drops were taken at a frequency of one drop every 2 s, and, for each surface tension value, about 15 images were taken.

In order to study the influence of the drop volume on the surface tension of polypropylene at 240 °C, a drop of polypropylene with the smallest volume was first formed in the experimental cell and analyzed as a function of time. Once the drop had reached mechanical equilibrium, its volume was increased and time was allowed for mechanical equilibrium to occur with this new value of the drop volume. This operation was then repeated for up to five different values of the volume. It was impossible to repeat the operation for more than five different values of the volume using the same drop, as the drop suffered thermal degradation.

Calculation of surface tension

The calculation of the surface tension from the drop profile consisted of four steps: edge detection, correction for optical anisotropy, obtaining the radius of curvature at the apex, robust shape comparison between the experimental and theoretical profile solution of the Bashforth and Adams equation.

Edge detection

Images of the drop were obtained and digitalized by a frame grabber in a Pentium II computer. Edge detection of the drops was then performed using the commercial software Global Lab Image. The contour of the drop consisted of the last pixel with a gray level higher than the threshold value.

Correction of optical anisotropy

A commercial stage micrometer (0.5 mm) square reticule was used in order to calibrate the optical system both horizontally and vertically, the perspective, and the offset of the image. The calibration procedures yielded different values of the optical enlargement in the horizontal and vertical directions. In order to take into account the anisotropy in the optical enlargements, a calibration procedure had to be developed. After digitalization, the coordinates of the drop (in pixels) were transformed according to

$$\begin{bmatrix} x_{\text{true}} \\ y_{\text{true}} \\ 1 \end{bmatrix} = \begin{pmatrix} a & b & X_0 \\ c & d & Y_0 \\ U & V & 1 \end{pmatrix} \begin{bmatrix} x_{\text{pixel}} \\ y_{\text{pixel}} \\ 1 \end{bmatrix}, \tag{5}$$

where $(x_{\text{true}}, y_{\text{true}})$ corresponds to the true coordinates of one point of the profile of the drop and $(x_{\text{pixel}}, y_{\text{pixel}})$ corresponds to the coordinates of that point in the digitalized image. The parameters a, b, c, and d cause a rotation and change the scale of the image. X_0 and Y_0 cause a translation of the image, and U and V correct the perspective (an inclination) in the image.

The first and third matrixes correspond to the corrected and uncorrected coordinates. The second matrix was determined by the calibration procedure, and it is called the pixel-to-real transformation matrix. When the pixel-to-real calibration matrix was known, the aspect ratio correction could be easily determined.

The calibration procedure was tested using stainless steel balls of known dimensions with a diameter of 3.016 ± 0.002 mm. These balls were considered as perfectly spherical. The dimensions of the balls were measured with different optical enlargements. The diameter in pixels of the sphere measured in the y direction versus that measured in the x direction for different optical enlargements is presented in Fig. 2. The squares represent the diameter after optical correction and the circles represent those before optical correction. For both cases, the data can be fitted to a straight line. The equations of the best fit of the data obtained by least-squares regression for both lines are shown on the graph. It can be seen that for balls with corrected optical anisotropy the angular coefficient is 0.997 and that for balls without correction the angular coefficient is around 0.97. These results show that the calibration procedure was necessary and efficient to correct for the optical anisotropy of the optical enlargement. Also, those results seem to indicate that a calibration for one magnification can be used for others magnifications (see values of r^2). It is interesting to mention that the optical anisotropy is apparently caused by the software/hardware (includes frame grabber) system, because when the optical system was turned 90°, the results were not altered.

If the calibration is not performed, when the magnification of the image is, for example, 1,346.2 pixels cm^{-1} along the x-axis, it is 1,306.4 pixels cm^{-1} along the y-axis. Therefore, if the calibration procedure is not performed, a drop image captured by the frame grabber will be flattened along the y-axis, leaving the drop shape more circular. An aspect ratio, f, which is the ratio between magnifications along the x-axis and along the y-axis can be defined. For the values of the optical enlargement reported here f is 1.030 when the calibration procedure is not performed and 1.00 when the calibration procedure is performed.

Obtaining the radius of curvature at the apex

Once the coordinates of the drops had been corrected for optical anisotropy, the radius of curvature at the apex of the drop,

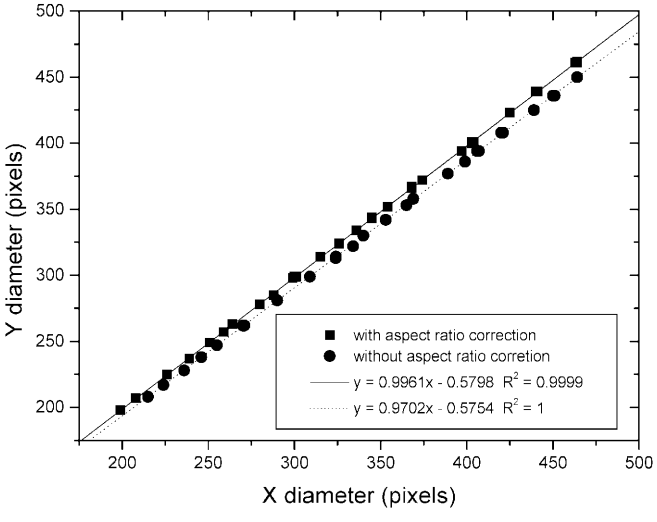

Fig. 2. Diameter of calibration sphere (pixels) measured along the y direction versus that measured along the x direction

necessary for the evaluation of the surface tension (Eq. 2), was evaluated. In many works, the value of the radius of curvature at the apex of the drop is taken as the distance between the apex and the center of the diameter as shown in Fig. 3a. In the case of longer drops, as shown in Fig. 3b, the values of the radius at the apex are overestimated, consequently overestimating the values of the surface tension. In this work, a special routine was written in order to evaluate the radius of curvature at the apex. Once the edge detection has been performed, the symmetry axis of the drop is determined. The intersection $I(X_I, Y_I)$ between the drop profile and the symmetry axis was also determined. Circles of different radius were superposed on the maximum number of points around the apex. The radius of the circle that superposes on the maximum number of points is taken as being equal to the radius of curvature of the drop at the apex, as shown in Fig. 3b.

Robust shape comparison

In order to infer the surface tension from the drop profile, a robust shape comparison between the experimental profile and the theoretical profile found by solving the Bashforth and Adams equation by a fourth-order Runge–Kunta method was used. The robust shape comparison consists of an optimization on five parameters: three parameters for alignment of the imaging system to the coordinate system of the dimensionless drop, the magnification factor of the drop, and the scaling factor B. The optimization was performed using around 100 points of the experimental drop profile that were chosen according to procedures described by Anastasiadis and coworkers [1, 2, 3] and Rotenberg et al. [25]. The optimized value of B was then used to calculate the surface tension using Eq. (2). The algorithms have been described in more detail elsewhere [7].

Results and discussion

The value of the shape factor returned by the shape comparison program are shown in Fig. 4 as a function of the drop volume for drops of glycerol. It can be seen that the shape factor is a decreasing function of the drop volume, corroborating the results of Huh and Reed [29].

The value of the shape factor returned by the shape comparison program is shown in Fig. 5 as a function of D_s/D_e (where D_e is the equatorial diameter and D_s is the diameter at a height D_e from the apex of drop) for all the drops of glycerol studied in this work for all the different drop volumes. It can be seen that two regions can be observed. For higher values of B (corresponding to small drop volumes), B seems to be an increasing function of D_s/D_e, and does not follow the equation of Huh and Reed. For lower values of B (corresponding to bigger drop volumes), B decreases as a function of D_s/D_e. The reason for having two different behaviors in the curve of B versus D_s/D_e may originate from the definition of D_s. The value of D_s/D_e, D_s, and D_e are shown in Fig. 6 as a function of the drop volume for a drop of glycerol. It can be seen that D_s is constant for drop volumes

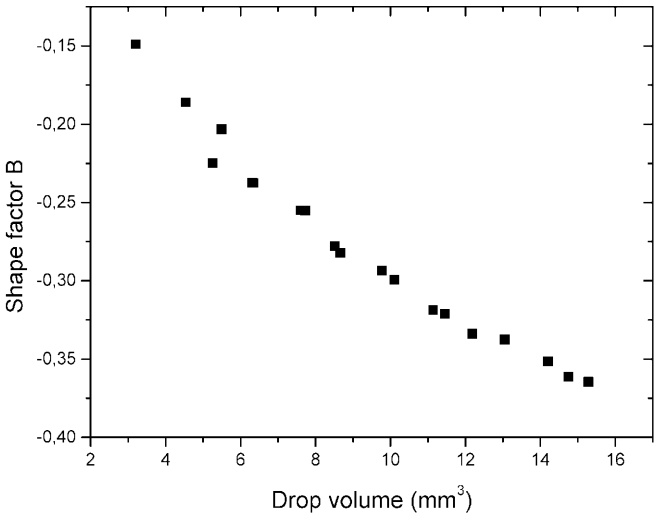

Fig. 4. Shape factor returned by the shape comparison program as a function of drop volume for drops of glycerol

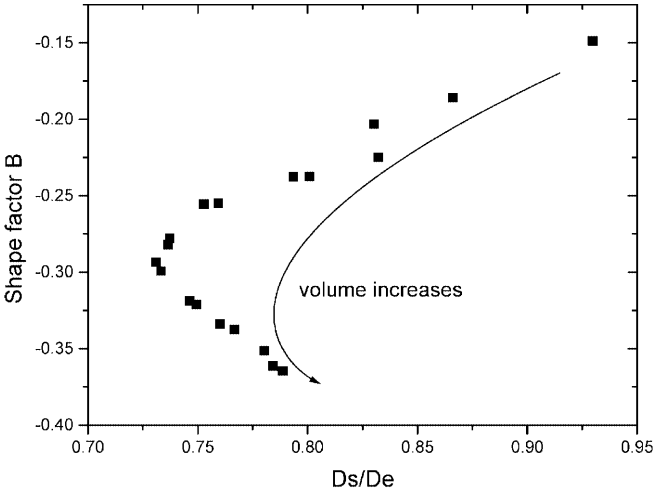

Fig. 5. Shape factor returned by the shape comparison program as a function of D_s/D_e for drops of glycerol (where D_e is the equatorial diameter of the drop and D_s is the diameter at a height D_e from the apex)

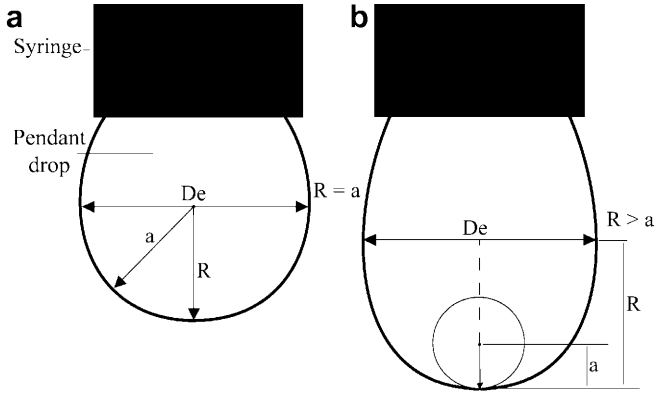

Fig. 3. Evaluation of the radius of curvature at the apex of a pendant drop for **a**) small drops and **b**) large drops

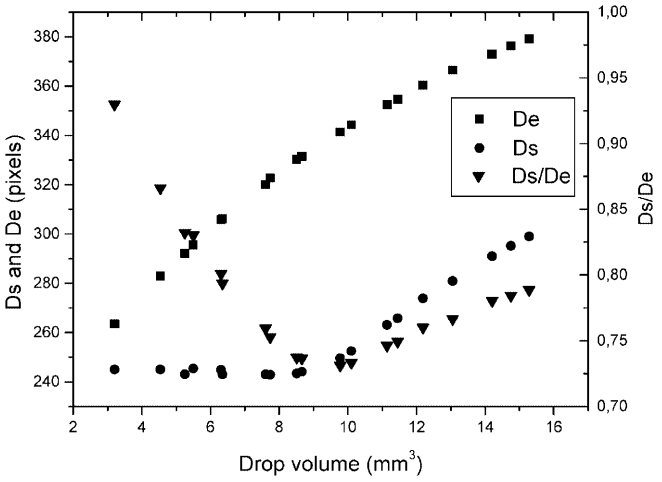

Fig. 6. D_s/D_e, D_s, and D_e as a function of drop volume for a drop of glycerol

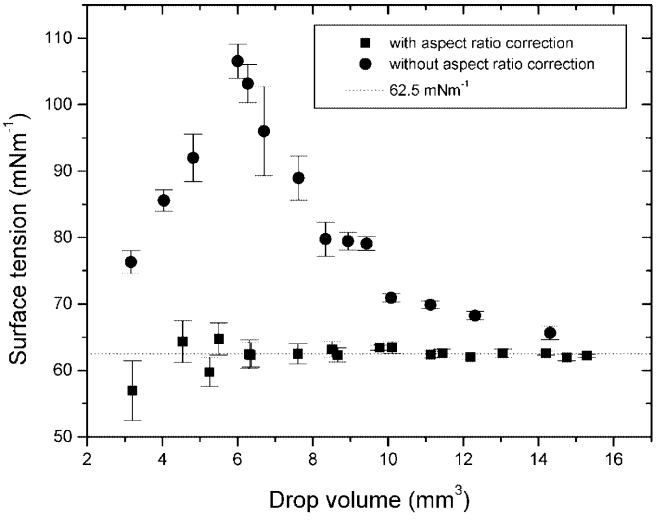

Fig. 7. Surface tension of glycerol as a function of drop volume with constant optical enlargement for all the drop images

ranging from 3 to 9 mm^3. For drop volumes larger than 9 mm^3, D_s increases with increasing drop volume. D_s is defined as the drop diameter measured horizontally at a distance D_e from the apex of the drop. For small drops, it is not possible to measure D_s and the value returned by the program is, in fact, the diameter of the syringe. For longer drops, D_s is located inside the drop.

The values of B as a function of $S = D_s/D_e$, once D_s could be measured along the drop profile, were fitted empirically to a polynomial. The best fit was

$$B = 182.51757 - 717.84332S + 940.5431S^2 - 411.2906S^3.$$

This fit was similar to the one obtained by Lin et al. [49] and Huh and Reed [29].

It can be seen that the use of the equations of Lin et al. or Huh and Reed can provide a good first approximation for large drops, but these equations fail for small drops (drops for which D_s can be located inside the needle).

The surface tension of glycerol is presented in Fig. 7 as a function of the drop volume with a constant optical enlargement for all the drop images. The squares represent the data obtained without correcting for optical anisotropy and the circles represent the data obtained once the anisotropy in the optical enlargements has been taken into account. The values presented in Fig. 7 represent the average obtained from the analysis of 15 different drops. It can be seen that when the optical anisotropy is taken into account, the surface tension is independent of drop volume and corroborates the value in the literature, i.e. 62.5 mNm^{-1} [52]; however, when the optical anisotropy is not taken into account, the surface tension is a decreasing function of drop volume.

A comparison between the shape factor B and the drop radius of curvature at the apex for drops profiles of glycerol with and without aspect ratio correction is shown in Figs. 8 and 9, respectively. It can be seen that the absolute value of B and the radius of curvature at the apex are respectively smaller and larger for drops profiles that were not corrected for optical anisotropy. These two factors could result in an overestimation of the value of surface tension (Eq. 2).

The surface tension of polypropylene is presented in Fig. 10 as a function of the time of the experiment. Drops of five different volumes were studied. The data obtained without correction for optical anisotropy are presented in Fig. 10a and the data with correction are presented in Fig. 10b. It can be seen that for each volume studied it takes around 50 min for the drop to reach mechanical equilibrium. After that, the drop reaches

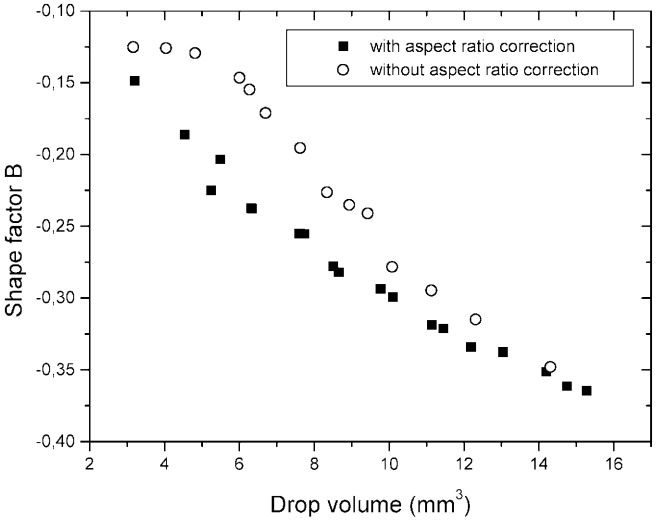

Fig. 8. Shape factor of drops of glycerol as a function of drop volume

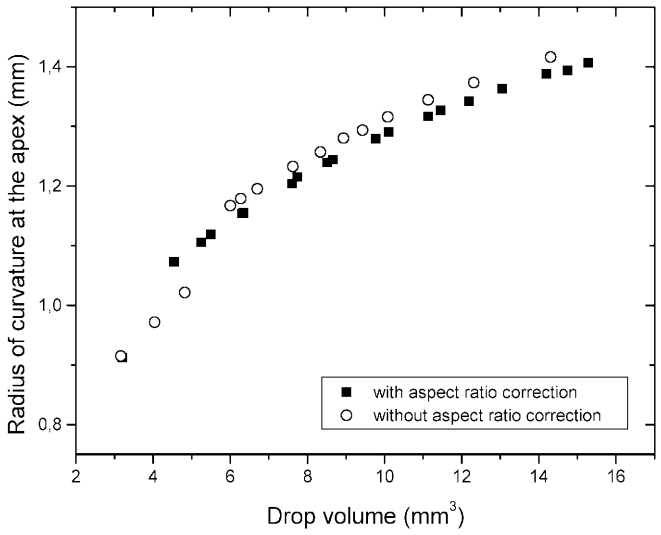

Fig. 9. Radius of curvature at the apex of drops of glycerin as a function of drop volume

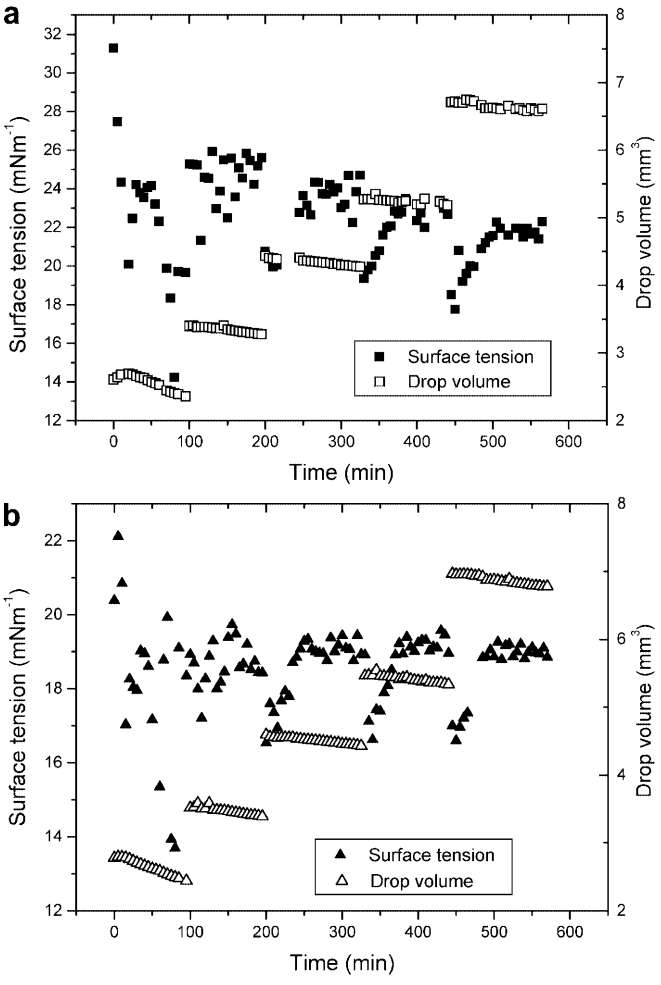

Fig. 10. Surface tension of polypropylene at 240 °C as a function of the time of the experiment **a**) without correction for the aspect ratio, f, and **b**) with correction for the aspect ratio

mechanical equilibrium and the surface tension stays constant as a function of time. The surface tension of polypropylene at 240 °C (obtained when the drop had reached mechanical equilibrium) is presented in Fig. 11 as a function of drop volume. The squares correspond to surface tension obtained when the optical correction was performed and the circles correspond to the surface tension obtained when the optical correction was not performed. It can be seen that when the optical correction is performed, the surface tension of polypropylene does not depend on the drop volume and corroborates the values in the literature [46]; however, when the optical correction is not performed, the surface tension is a decreasing function of the volume. These results corroborate the results given earlier for glycerol: the occurrence of a dependence of the surface tension on the drop volume does not seem therefore to depend on the surface tension, showing that it is probably related to the lack of optical correction for anisotropy.

The variation of the surface tension with the drop volume has already been reported in the literature [27, 49, 51, 53]. In particular, Lin et al. [49] evaluated the surface tension of different liquids with surface tensions varying from 20 to 70 mNm^{-1} with different syringe radiuses. The authors observed that the surface tension obtained from their drop profile analysis increased when the volume of the drop increased and reached the tabulated value of the surface tensions for a range of volumes extending to the maximum drop volume. The difference between the results obtained by Lin et al [49] and those presented here can be explained by the difference in anisotropic magnification factor. In the case of the experiments reported here, f was greater than 1, whereas in the case of Lin et al. [49], f was smaller than 1. The surface tension of glycerol is shown in Fig. 12 as a function of the drop volume when $f<1$, $f=1$, and $f>1$. The values of the surface tension obtained when $f<1$ were obtained by analyzing experimental profiles that had been purposely distorted using the transformation shown in Eq. (5) twice. It can be seen that when $f<1$, the surface tension is an increasing function of the drop volume, when $f=1$ the surface tension does not seem to vary with the drop volume, and when $f>1$ the surface tension is a decreasing function of the drop volume. Similar results were obtained for polypropylene.

The results presented in Figs. 7 and 11 also indicate that the standard deviation of the surface tension results obtained by drop-shape comparison is greater for smaller drops than larger ones, for the same optical enlargement. This is probably due to the smaller number of points to define the pendant drop profile of a smaller drop and this involves greater imprecision. Typically, for an optical enlargement of 1,346.2 pixel cm^{-1} along the x-axis, drops with a volume of 5.47 mm^3 had a drop

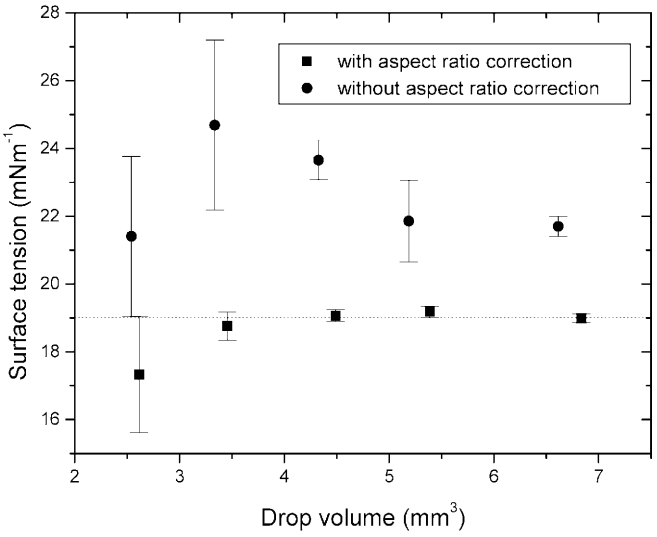

Fig. 11. Surface tension of polypropylene at 240 °C as a function of drop volume

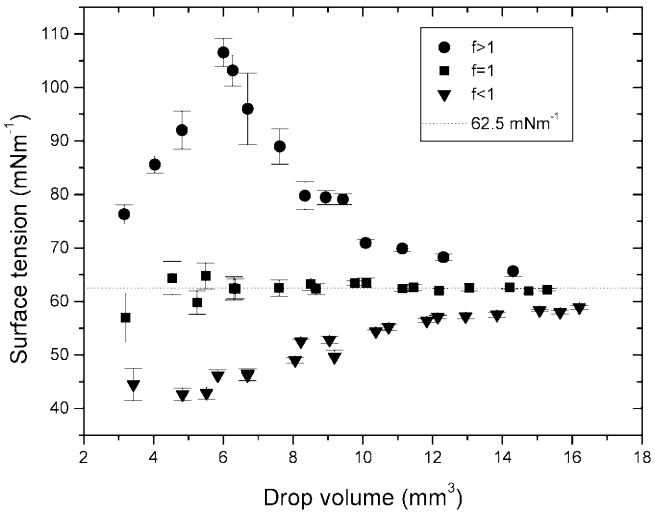

Fig. 12. Surface tension of glycerol as a function of drop volume when $f < 1$, $f = 1$, and $f > 1$

profile formed by 466 points, whereas drops with a volume of 15.1 mm^3 had a drop profile formed by 726 points. The high standard deviation for small drops can therefore be decreased if a larger optical enlargement is used. These results corroborate those obtained by Song and Springer [18], who observed that the standard deviation was smaller for drops with larger values of B.

Conclusions

In this work, it was verified that the optical anisotropy of digitalization systems used for pendant drop analysis can result in a large error in surface tension determination. Therefore, a calibration procedure to take into account this optical anisotropy was developed. This calibration procedure could be used for the optical system for every magnification. It was shown that the optical distortion could be attributed to the software/hardware (including frame grabber) used to do the image analysis.

The surface tensions of glycerol at 25 °C and polypropylene at 240 °C were evaluated using the pendant drop method. Drops of different volumes, ranging from 3 to 16 mm^3 for glycerol and from 2.5 to 7 mm^3 for polypropylene were considered for surface tension analysis. It was shown, for both liquids studied in this work, that when the calibration procedure was not performed the surface tension was a function of the drop volume and that when the calibration procedure was performed the surface tension did not depend on the drop size and it corroborated the values in the literature. It was shown that the dependence of the surface tension on the drop volume reported in the literature may be due to the lack of calibration for optical anisotropy.

Acknowledgements The authors thank FAPESP (grants 94/03351-6, 97/06071-2, 99/12332-9), Rodrigo Viana, and Osvaldo Mitsuyuki Cintho for helping performing some of the experiments.

References

1. Anastasiadis SH, Gancarz I, Koberstein JT (1988) Macromolecules 21:2980
2. Anastasiadis SH, Gancarz I, Koberstein JT (1989) Macromolecules 22:1449
3. Anastasiadis SH, Chen JK, Koberstein JT, Siegel AF, Sohn JE, Emerson JA (1987) J. Colloid Interface Sci 119:55
4. Demarquette NR, Kamal MR (1994) Polym Eng Sci 34:1823
5. Kamal MR, Demarquette NR, Lai Fook RA (1994) Polym Eng Sci 37:813
6. Cho D, Hu W, Koberstein JT, Lingelser JP, Gallot Y (2000) Macromolecules 33:5245
7. Arashiro EY, Demarquette NR (1999) J Appl Polym Sci 74:2423
8. Menke TJ, Funke Z, Maier RD, Kressler J (2000) Macromolecules 33:6120
9. Nam KH, Cho JC, Jo WH (1995) Polym J 27:904
10. Liang H, Xu R, Favis BD, Shreiber HP (2000) J Polym Sci Polym Phys 38:2096
11. Fleischer CA, Koberstein JT, Krukonis V, Wetmore PA (1993) Macromolecules 26:4172
12. Fleischer CA, Morales AR, Koberstein JT (1994) Macromolecules 27:379
13. Xing P, Bousmina M, Rodrigue D, Kamal MR (2000) Macromolecules 33:8020

14. Chen CC, White JL (1993) Polym Eng Sci 33:923
15. Jo WH, Nam KH, Cho JC (1996) J Polym Sci Polym Phys 34:2169
16. Kwok DY, Cheung LK, Park CB, Neumann AW (1998) Polym Eng Sci 38:757
17. Song B, Springer J (1996) J Colloid Interface Sci 184:64
18. Song B, Springer J (1996) J Colloid Interface Sci 184:77
19. Runke T, Song B, Springer J (1994) Bunsenges Phys Chem 98:508
20. Shimizu RN, Demarquette NR (2000) J Appl Polym Sci 76:1831
21. Jimbo I, Cramb AW (1992) ISIJ Int 32:26
22. Jon DI, Rosano HL, Cummins HZ (1986) J Colloid Interface Sci 114:330
23. Terriza JAH, Lopera JFG, Escamilla PLL, Allah CA, Vílchez MAC (1999) Colloids Surf A 156:579
24. Voigt A, Thiel O, Williams D, et al (1991) Colloids Surf 58:315
25. Rotenberg Y, Boruvka L, Neumann AW (1983) J Colloid Interface Sci 93:169
26. Jennings JW, Pallas NR (1998) Langmuir 4:959
27. Lin SY, Hwang HF (1994) Langmuir 10:4703
28. Bashforth S, Addams JC (1982) An attempt to test the theory of capillary action. Cambridge University Press and Deighton, Bell and Co, London
29. Huh C, Reed RL (1991) J Colloid Interface Sci 91:472
30. Ramos L, Redner RA, Cerro RL (1993) Langmuir 9:3691
31. Stauffer E (1965) J Phys Chem 69:1933
32. Andreas JM, Hauser EA, Tucker WB (1938) J Phys Chem 42:1001
33. Fordham S (1948) Proc R Soc Lond Ser A 149:1
34. Roe RJ (1970) J Phys Chem 72:2013
35. Carla M, Cecchini R, Bordi S (1991) Rev Sci Instrum 62:1088
36. Girault HH, Schiffrin DJ, Smith BDV (1984) J Colloid Interface Sci 101:257
37. Girault HH, Schiffrin DJ, Smith BDV (1982) J Electroanal Chem 137:207
38. Hansen FK, Rodsrud G (1991) J Colloid Interface Sci 141:1
39. Rienstra SW (1990) J Eng Math 24:193
40. Prokop RM, del Rio OI, Niyakan N, Neumann AW (1996) Can J Chem Eng 74:534
41. Skinner FK, Rotenberg Y, Neumann AW (1998) J Colloid Interface Sci 130:25
42. Alvarez JM, Amirfazli A, Neumann AW (1999) Colloids Surf 156:163
43. Amirfazli A, Graham-Eagle J, Pennell S, Neumann AW (2000) Colloids Surf 161:63
44. Augsburg A., Grundke K, Pöschel K, Jacobasch HJ, Neumann AW (1998) Acta Polym 49:417
45. Miller R, Treppo S, Voigt A, Zingg W, Neumann AW (1993) Colloids Surf 69:203
46. Wulf M, Michel S, Grundke K, Del Rio OI, Kwok DY, Neumann AW (1999) J Colloid Interface Sci 210:172
47. Pallas NR, Harrison Y (1990) Colloids Surf 43:169
48. Hayami Y (1996) Colloid Polym Sci 274:643
49. Lin SY, Wang WJ, Lin LW, Chen LJ (1996) Colloids Surf 114:31
50. Adão MH, Saramago B, Fernandes AC (1998) Langmuir 14:4198
51. Lin SY, Chen LJ, Xyu JW, Wang WJ (1995) Langmuir 11:4159
52. Dean JA (1992) Lange's handbook of chemistry. Mc Graw-Hill, New York
53. Alam K, Kamal MR (1999) Antec 1999, New York, pp 1955–1959